sustainability

MDPI

Article

Simulation Optimization of an Industrial Heavy-Duty Truck Based on Fluid–Structure Coupling

Xinyu Song [1,2], Fang Cao [1,2,*], Weifeng Rao [1,2] and Peiwen Huang [1,2]

[1] School of Mechanical Engineering, Qilu University of Technology (Shandong Academy of Sciences), Jinan 250353, China
[2] Shandong Institute of Mechanical Design and Research, Jinan 250031, China
* Correspondence: caofang@qlu.edu.cn

Abstract: In order to realize the sustainable development of the field of automotive industrial engineering and reduce the emissions of heavy-duty trucks (HDTs), a simulation analysis method that combined fluid–structure coupling and a discrete phase model was proposed in this study. The pressure, velocity, and other parameters of an HDT air filter and its cartridge were analyzed by using CFX and the Static Structure module in the ANSYS software. The results showed that under six different flow rates, the error between the simulation results and the test results was basically less than 3% (the maximum error was 3.4%), and the pressure distribution of the fluid in the air filter was very uneven, leading to a severe deformation of 3.51 mm in the filter element. In order to reduce the pressure drop of the air filter and the deformation of the filter element, the position of the air inlet duct, the height of the filter element, and the number of folds of the air filter were optimized in this study. The optimization results showed that when the rated flow was 840 m^3/h, compared with the original structure, the pressure drop of the air filter was reduced by 445 Pa, the maximum deformation of the filter element was reduced by 54.1% and the average deformation is reduced by 39.8%. After the optimization, the structural parameters of the air filter were as follows: the position of the air inlet moved down 126 mm along the shell, the filter height was 267 mm, and the pleat number of the filter element was 70. The simulation method and optimization design method of an air filter based on fluid–structure interaction presented in this study can be used to reduce the pressure drop, improve the engine performance, and reduce the amount of harmful emissions.

Keywords: sustainable development; fluid–structure coupling; air filter; simulation optimization

check for updates

Citation: Song, X.; Cao, F.; Rao, W.; Huang, P. Simulation Optimization of an Industrial Heavy-Duty Truck Based on Fluid–Structure Coupling. *Sustainability* **2022**, *14*, 14519. https://doi.org/10.3390/su142114519

Academic Editors: Babek Erdebilli (B.D Rouyendegh) and Erfan Babaee Tirkolaee

Received: 13 October 2022
Accepted: 2 November 2022
Published: 4 November 2022

Publisher's Note: MDPI stays neutral with regard to jurisdictional claims in published maps and institutional affiliations.

Copyright: © 2022 by the authors. Licensee MDPI, Basel, Switzerland. This article is an open access article distributed under the terms and conditions of the Creative Commons Attribution (CC BY) license (https://creativecommons.org/licenses/by/4.0/).

1. Introduction

Due to the requirements of sustainable industrial engineering, the automotive industry is constantly innovating and changing. As part of this trend, small- and medium-sized passenger vehicles have been gradually electrified to reduce energy consumption and air pollution. However, cargo vehicles, especially heavy-duty trucks (HDTs), still need diesel to run. Compared with cars, although the number of HDTs is small, they have a greater impact on NO_x and particulate matter (PM) emissions. The pressure drop of an air filter is the key factor that determines engine exhaust emission. An excessive pressure drop will hinder the flow of air into the cylinder, resulting in higher engine fuel consumption and more serious pollution. Studies showed that 70% of the early damage to an engine is caused by the air filter not being replaced in time or not realizing its filtering function [1].

In a study of pressure drop on engine performance, Tadeusz Dziubak and Karczewski Mirosław showed through experiments that an increase in pressure drop will increase the fuel consumption and exhaust smoke of the internal combustion engine [2]. Many scholars used simulations to study the actual working conditions of air filters and obtain data that may be difficult to achieve with experimental methods [3–7]. Li Qiang et al. proposed a linear empirical equation to predict the pressure drop of air filters, and the accuracy was

verified using experimental data [8]. In Jeong-Eui Yun's study, in order to improve the centrifugal dust removal effect of the pre-cleaner, the structure of the inclination angle and air channel position angle was optimized [9]. Birtok-Baneasa greatly reduced the airflow power loss, increased the suction efficiency, and enhanced the dust capture rate by simplifying the air filter housing so that the filter element is in direct contact with the air [10]. Gang Wang focused on increasing the cross-sectional area of the air filter inlet duct and increasing the diameter of the guide volute while reducing its number; their results showed that the pressure drop was reduced by 24.96% in comparison to the original scheme [11]. Sabry Allam studied the influence of different parameters of a pleated filter element on the engine. Experimental and numerical simulation results showed that the sine-wave-shaped pleated filter element produced a lower pressure drop [12]. Arun Kumar Pardhan produced nonwoven filter elements with different fiber densities and measured the pressure drop and filtration loss under the same conditions [13]. Ajay Kumar Maddineni introduced a numerical method for estimating flow fields and pressure drops within pleated air filter systems that are commonly used in automotive engine air intakes [14]. Tadeusz Dziubak and Leszek Bąkała proposed a two-stage intake filtration system for special vehicle internal combustion engines, providing a comparative analysis of the filtration performance of the return tube and vortex tube separators (VTS) [15]. Diol.-Ing Mario Rieger designed a circular pleated filter element with a semicircle connecting both sides of the plane, which did not reduce the filter area but greatly reduced the space occupied by the filter element; the corresponding air filter volume was greatly reduced, which mitigated the poor performance of the compact air filters [16]. Many scholars have also done a lot of research on fluid–structure interaction and porous media, and the numerical simulation methods in this area are more accurate [17–20].

Via a comprehensive analysis of the current research status and progress, it can be seen that scholars' research on air filters mainly focused on the simulation optimization of the air filter shell shape and the analysis of filter paper material characteristics. However, there are few studies on HDT air filters in industrial engineering and few studies on filter element deformation and wear caused by flow field flow in air filters. Therefore, a simulation analysis method that combined unidirectional fluid–structure coupling and a discrete phase model was applied to an HDT air filter in this study, and the experimental results showed that the simulation method was very suitable for the research of HDT air filters (the data error of the test and simulation was basically controlled to within 3%). Based on the fluid–structure coupling simulation method, the influence of the inlet duct position on the pressure drop and filter element deformation in the air filter was analyzed, and on this basis, the filter element height and filter element fold number were co-simulated and optimized. The optimization results can be used in the research of the heavy truck industry, such as flow uniformity, vibration, and noise.

2. Literature Review and Critique

2.1. Literature Review

At present, scholars' research on air filters can be summarized in two aspects. First of all, the shell structure and the layout of the inlet and outlet of an air filter are feasible to optimize to improve the structure of the air filter. Many scholars also optimized the structure of air filters from this perspective.

Al-Sarkhi et al. added a catheter at the entrance of an air filter and measured the velocity field of the air filter with the catheter through an LAD (laser Doppler anemometer). They found that the velocity field of the air filter became more uniform after the catheter was added [21]. Zhao Shuen et al. changed the end pipe at the outlet of the air filter from a straight corner to a smooth chamfer corner and moved the inlet pipe down at the same time. After numerical simulation of the improved air filter, they found that its pressure loss was reduced by 7.97% [22]. Li Rongjun added a dust removal structure to the bottom opening of an air filter and found through experiments that increasing the dust removal structure could not only improve the filtration efficiency of the air filter but also reduce the

pressure loss of the air filter [23]. Bartolo et al. analyzed the flow field characteristics of an air filter shell of a four-cylinder engine through numerical simulations and measured its velocity field through an LAD (laser Doppler anemometer). The results measured using the LAD were compared with the simulation results and they were found to be basically consistent. It shows that the numerical simulation method for an air filter of a four-cylinder engine is reasonable [24]. Lu Jinjun et al. optimized the shape and structure of an air filter with a blade ring type for a heavy off-road vehicle through numerical simulations. They found that the optimized air filter could meet the design requirements of the product in a smaller volume, saving the installation space of the air filter in the car, and the pressure loss of the improved air filter was lower than that of the original air filter [25].

The second aspect is about the air filter element research. The flow of air in the filter element is complicated because it is turbulent flow in the upstream and downstream regions of the filter element, but laminar flow in the filter element [26]. Li Jia et al. analyzed the angle of the air filter element and found that when the angle of the filter element is less than 3°, the pressure loss of the air filter rises sharply. When the angle of the filter element is greater than 5°, there is no significant change. When the angle of the filter element is greater than 4°, the service life of the filter element will be shortened. Therefore, the appropriate angle of the filter element is 3−4° [27]. Fotovati et al. also studied the angle of the filter element and found that the optimal angle range to minimize the pressure drop was 10−15° [28]. Tan Yongnan analyzed the influence of parameters such as the fold number, inner diameter, and outer diameter of the filter element on the pressure drop and velocity field of an air filter. The results show that the pressure drop of the air filter increased with an increase in fold number and outer diameter [29]. Binns et al. studied the pressure drop of the filter element of a racing car under different turbulence models, such as a planar porous media model and coupled porous media model, and compared the simulation results with the experimental results, which showed that the coupled porous media model was the most consistent with the experimental results [30].

2.2. Literature Summary

The literature review is very helpful for the research of air filters for HDTs. Through reading the existing literature, it can be seen that there are shortcomings in the research of air filters in some aspects. First of all, the research object of current scholars is mainly household vehicle air filters. There is little research on the air filters of heavy-duty trucks, especially those working in extremely harsh environments. Second, the effect of the flow field flow on the cartridge was not considered in previous studies. Fluid in the air filter will impact the filter element, causing deformation and wear of the filter element, resulting in a decrease in the service life and filtration performance of the filter element; therefore, research in this direction is also important.

For these reasons, this study proposed a fluid–solid coupling simulation method for HDT air filters and verified the accuracy of the simulation method through experiments. Then, the air filter was further optimized regarding three aspects: the intake duct position, filter element height, and pleat number. The optimization objectives were to reduce the air inlet resistance and to reduce the deformation of the filter element.

3. Governing Equations

3.1. Fluid Governing Equations

The air filter investigated in this study contained an incompressible flow, and the heat exchange was so small that it could be ignored; therefore, the law of conservation of energy was not considered in this study. Further, the filter element was simulated using a porous medium model in the fluid domain. The porous medium model in the CFX simulation software is an empirical model established based on the N-S equation and the generalized

Darcy's law, including an anisotropic loss model. In the porous media region, the governing equations represented by the velocity U are as follows:

$$\text{Continuity equation}: \quad \frac{\partial}{\partial t}\cdot(\gamma\rho) + \nabla\cdot\left(\rho K' U\right) = 0 \tag{1}$$

$$\text{Momentum equation}: \quad \frac{\partial}{\partial t}(\gamma\rho U) + \nabla\cdot\left(\rho K' U U\right) - \nabla\cdot\left(\mu_{eff} K'\cdot\left(\nabla U + \left(\nabla U\right)^T\right)\right) = -\gamma R U - \gamma\nabla P \tag{2}$$

$$\text{Transport equation}: \quad \frac{\partial}{\partial t}(\gamma\rho\phi) + \nabla\cdot\left(\rho K' U\phi\right) - \nabla\cdot\left((D_A + D_t)K'\cdot\nabla\phi\right) = \gamma S \tag{3}$$

where γ is the bulk porosity and K' is the areal porosity; in this study, $K' = \gamma$. $R = (R_{ij})$ represents the impedance of the fluid in the porous medium; generally, it is a symmetric finite positive second-order tensor used to describe the possible anisotropic impedance. Impedance is expressed in CFX using the Darcy–Forchheimer law, which takes the form

$$-\frac{\partial P}{\partial x_i} = \frac{\mu}{K}U_i + K_{loss}\rho|U|U_i \tag{4}$$

where K is the permeability and K_{loss} is the resistance loss coefficient. In the porous media region in this study, the fluid Reynolds number was $Re < 10$, which satisfies the application conditions of Darcy's law; therefore, the resistance loss coefficient can be ignored.

3.2. Solid Governing Equations

The governing equation for solids that vibrate and move due to fluid flow is as follows:

$$M_s\frac{d^2r}{dt^2} + C_s\frac{dr}{dt} + k_s d_s + \tau_s = 0 \tag{5}$$

where M_s is the mass matrix, C_s is the damping matrix, K_s is the stiffness matrix, d_s is the displacement of the solid in m, τ_s is the stress acting on the solid in MPa, and t is the time in s.

3.3. Fluid–Structure Coupling Control Equation

In the fluid–structure coupling analysis, the fluid and solid at the coupling interface need to satisfy the corresponding conservation laws:

$$\tau_f\cdot n_f = \tau_s\cdot n_s \tag{6}$$

$$d_f = d_s \tag{7}$$

where τ_f and τ_s are the stresses of the fluid and solid, respectively, in MPa; d_f and d_s are the displacements of the fluid and solid, respectively, in m; and n_s and n_f are the micro-elements of the solid and fluid, respectively.

3.4. DPM Model Governing Equations

When a particle moves in a fluid, the force acting on the particle comes mainly from the velocity difference between the fluid and the particle. The expression of the force is

$$m_p\frac{du_p}{dt} = F_D + F_B + F_G + F_V + F_P + F_X \tag{8}$$

where t is the time, m_p is the particle mass, u_p is the particle velocity, F_D is the resistance, F_B is the Basset force, F_G is the gravitational force, F_V is the virtual mass force, F_P is the pressure gradient force, and F_X is the sum of other external forces.

In this study, due to the low concentration of particles in the flow field, the fluid velocity of the continuous phase was large, and there was a significant density difference between the continuous phase and the discrete phase; therefore, the virtual mass force, pressure gradient force, Basset force, Saffman force, and Magnus force were not considered. Hence, the basic equations of particle motion could be expressed as

$$\frac{dx_{pi}}{dt} = u_{pi} \tag{9}$$

$$\frac{du_{pi}}{dt} = \frac{3C_D\rho_f}{4\rho_p D_p}|u_s|u_s \tag{10}$$

where u_s is the slip velocity between the liquid phase and the particle phase, C_D is the drag coefficient related to the Reynolds number, ρ_f is the liquid density, ρ_p is the particle density, D_p is the particle diameter, and X_{pi} is the spatial coordinate position of the particle. It can be seen from the formula that, when a particle moves in a liquid, its trajectory is related to the particle diameter and density.

4. Numerical Simulation Method

4.1. Geometric Model

The research object of this study was an air filter of an HDT, which included a pleated filter element. In the 3D modeling process, certain structures that have limited influence on the simulation results were simplified; the final structure is shown in Figure 1. The internal fluid domain of the air filter was extracted using the "Geometry" preprocessing software, and the required fluid domain and filter element solid domain models were obtained. Among them, only the upper and lower sealing rings of the filter element played the role of affixing the paper filter element, which had little effect on the simulation results and would increase the complexity involved in meshing. Therefore, the sealing rings at both ends of the filter element were deleted, and the results are shown in Figure 2.

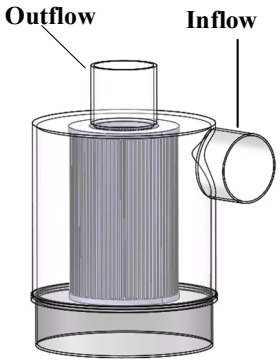


Figure 1. Overall structure of the air filter.

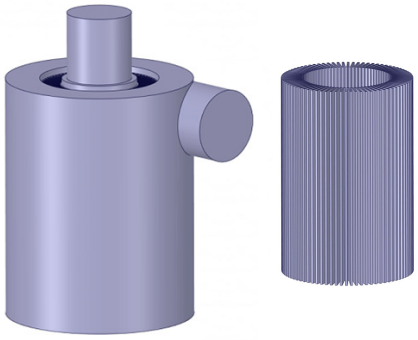


Figure 2. Air filter internal fluid domain and filter element solid domain model.

4.2. Grid Establishment

In this study, the mesh was generated using "ANSYS meshing" software. The solid domain was divided separately using unstructured grids due to the large number of filter pleats, generating a total of 712,800 nodes and 100,800 grids. The inner fluid domain of the air filter was divided using a polyhedral mesh. A polyhedral mesh is quickly generated, has high adaptability to complex structural shapes, and is more efficient than unstructured meshes in terms of calculation speed. In the fluid domain, a total of 394,800 nodes and 446,189 meshes were generated. The quality of the generated mesh was checked; there was no negative volume, the average orthogonal mass was 0.76, the smoothness was good, and the mesh quality was high. The divided HDT air filter internal fluid domain and solid domain meshes are shown in Figure 3.

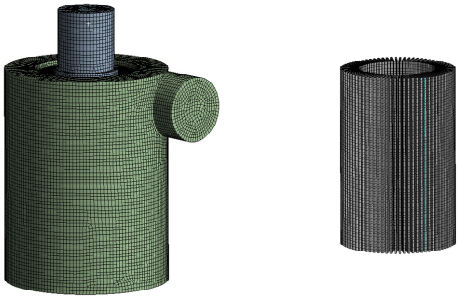


Figure 3. Air filter fluid domain and cartridge solid domain grid.

4.3. Boundary Conditions and Material Properties

4.3.1. Fluid Domain

The focus of this study was on the flow process of fluids inside an HDT air filter, where the continuous phase was air. According to the actual working situation, the gravitational acceleration of the fluid in the air filter was about 9.8 m/s^2, the inlet of the fluid domain was set as a pressure inlet, the inlet gauge pressure was 100,300 Pa, and the outlet was set as a velocity outlet; the velocity value was calculated from the volume flow rate at the outlet of the air filter in the test:

$$V = Q_v \times S \tag{11}$$

where V is the air velocity at the outlet, Q_v is the constant flow rate, and S is the outlet area of the HDT.

The finite element parameters for the fluid part of the CFX module were set as shown in Table 1 below.

Table 1. The fluid part's finite element parameters.

Parameters:	Options	Numerical Value
Inlet	Pressure inlet	100,300 Pa
Outlet	Velocity outlet	29.7 m/s
Fluid	Air ideal gas	9.8 m/s^2 (gravity)
Porous media	Porosity rate	0.9

4.3.2. Solid Domain

During the linear static structural analysis of the solid domain model of the filter element, the filter element material was fiber paper, fixed supports were applied at both ends of the filter element and the surface of the filter element was set as the fluid–solid coupling interface. The air filter fluid domain analysis results obtained using the "CFX" software were imported into the "Static Structure" software as the pressure load conditions of the solid domain, as shown in Figure 4.



Figure 4. Pressure load and fixed supports for filter elements.

The finite element parameters for the solid part of the Static Structure module were set as shown in Table 2 below.

Table 2. The solid part's finite element parameters.

Parameters	Options	Numerical Value
Materials	Density	1.25 kg/m^3
	Poisson's ratio	0.307
	Young's modulus	18.9 GPa

4.4. Grid Independence Test

During simulation calculations, the quality and quantity of grids have a great influence on the accuracy and calculation efficiency of the simulation results. Only by guaranteeing a certain number of grids can a more accurate calculation result be obtained. To verify the accuracy of the results, the grid number of the model was divided into five levels—319,708, 446,189, 669,371, 1,087,546, and 1,577,248—and simulations were carried out. The pressure drop of inlet and outlet pressure was taken as the evaluation index. Figure 5 shows that the pressure drop varied with the number of grids; it can be seen that when the number of grids was greater than 4.0×10^5, the relative error of the calculation result was less than 4%, and the calculation result tended to be stable. However, increasing the number of meshes reduced the computational efficiency of the simulation and increased the computational time. Therefore, after comprehensively considering the relationship between the accuracy of the simulation results and the calculation efficiency, the number of simulation calculation grids was maintained between 5.0×10^5 and 8.0×10^5, which met the accuracy requirements of the simulated flow field.

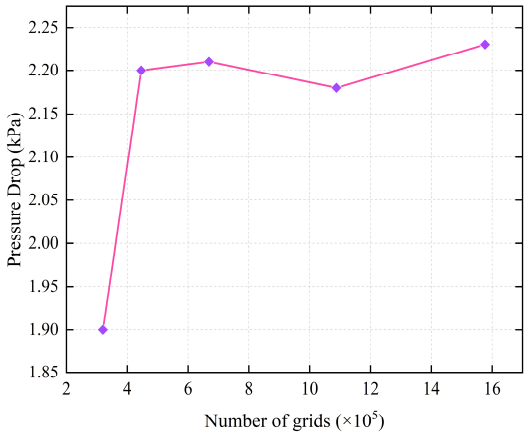
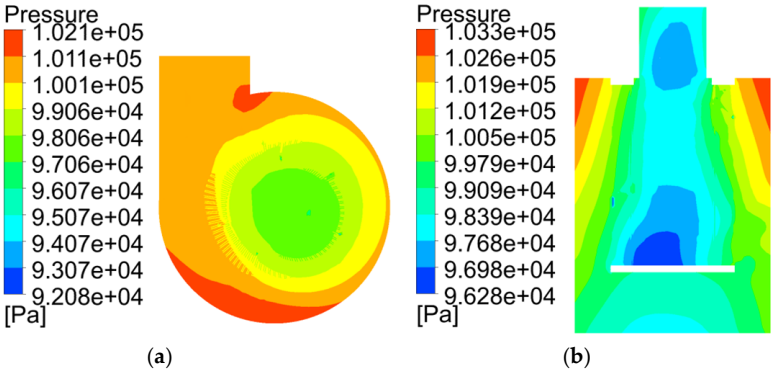


Figure 5. Variation in the pressure drop with the number of grids.

4.5. Simulation Results and Analysis

4.5.1. Pressure Field and Velocity Field Analysis

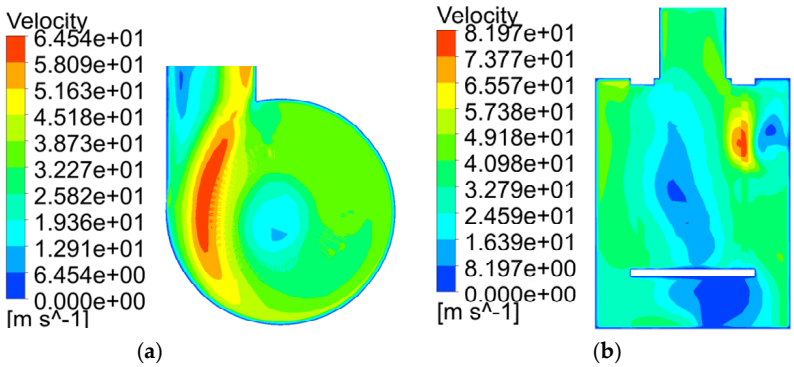
Figure 6 shows the flow field pressure distribution diagram of the original structure of the HDT air filter when the rated flow rate was 840 m^3/h. It is clear from Figure 6 that when the air flowed in from the air inlet, the airflow was directed to the left side of the filter element, resulting in a local pressure concentration on the left side of the filter element. Furthermore, the lower-left housing of the air filter was also greatly impacted by the fluid owing to the position of the air intake. The pressure on the filter element on the side away from the air inlet was smaller and more evenly distributed, but the airflow rate was lower and the working efficiency of the filter element was poor. In addition, the uneven pressure distribution of the air in the circumferential direction of the filter element will reduce the filtration efficiency of the filter element and shorten its service life. When the dust and impurities in the air are filtered and absorbed by the filter element, the resistance loss caused by the material of the filter element is large; therefore, the pressure generated is large. The outlet position experiences sub-atmospheric pressure, making it easy for air to flow out.



(**a**) (**b**)

Figure 6. Pressure distribution diagram of the original structure of the HDT air filter. (**a**) y = 0.48 m Z–X plane pressure distribution. (**b**) z = 0.2 m X–Y plane pressure distribution.

When the air enters the air filter, it can be seen from Figure 7 that there was an area of high fluid velocity at the connection between the air inlet and the housing (the highest velocity reached 82 m/s). When the engine is working normally, the filter element located in this area will be impacted by high-speed fluids for a long time, which will accelerate the wear and deformation of the filter element, causing the filter element to be damaged prematurely and shortening its service life. After the air passed through the filter element, the velocity was greatly reduced and remained relatively stable; however, due to the influence of the inlet position, the velocity distribution of the flow field inside the filter element was uneven, and the airflow accumulated at one side of the air filter.



(**a**) (**b**)

Figure 7. Velocity distribution diagram of the original structure of the HDT air filter. (**a**) y = 0.48 m Z−X plane velocity distribution. (**b**) z = 0.2 m X−Y plane velocity distribution.

4.5.2. Flow Field Streamline and Particle Trajectory Analysis

It can be seen from the streamline of the flow field in Figure 8 that the fluid passing rate of the filter element on the side near the intake pipe was higher, as it was affected by the position of the intake pipe, and more fluid flowed through the filter element and flowed out from the air outlet of the air filter. This area also exhibited local pressure concentration and the velocity values mentioned in the pressure and velocity analysis, which had a great impact on the overall working efficiency of the air filter. The flow of fluid in the air filter was relatively stable, with no large eddy currents.

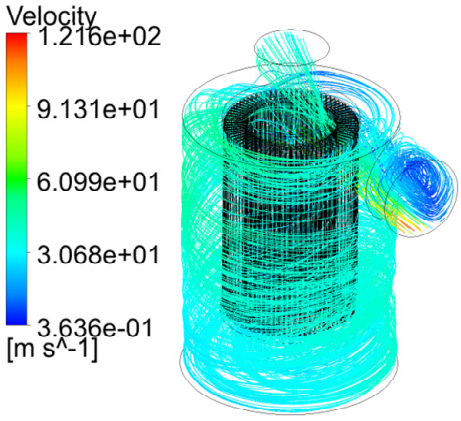


Figure 8. Air filter flow field streamline.

After the rough filtration of the front air intake system, most of the particulate dust was filtered and collected, and only particles with a diameter of lower than 10 μm entered the air filter cavity through the air intake port of the filter. In this study, the DPM model was used to calculate the trajectory of particles with an average diameter of 5 μm in the air filter of an HDT. As shown in Figure 9, the particles moved inside the air filter in the direction of the flow field, and the low-porosity air filter element filters adsorbed the particles, preventing them from passing through the inner cavity of the air filter and entering the engine. Finally, the particles were deposited at the bottom of the air filter under the action of gravity and were discharged from the dust outlet or collected by the dust-holding device, which restored the actual working conditions of the air filter.

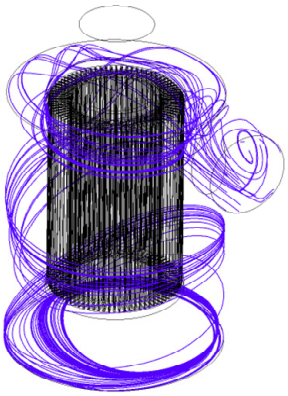


Figure 9. Air filter particle trajectory.

4.5.3. Deformation Analysis of Filter Element Based on the Fluid–Structure Coupling

In this study, through the simulation of the one-way fluid–structure coupling, the deformation of the filter element under the action of the flow field is shown in Figure 10. It can be seen from Figure 10 that the degree of deformation of the filter element in the circumferential direction was consistent with the distribution of the pressure value of the flow field. Owing to the uneven distribution of the pressure value in the flow field, the

filter element exhibited a large local deformation in the circumferential direction, and the maximum deformation amount reached 4.6 times the average deformation amount. Excessive deformation of the filter element will lead to premature damage, shorten its service life, and reduce the overall filtration efficiency of the air filter.

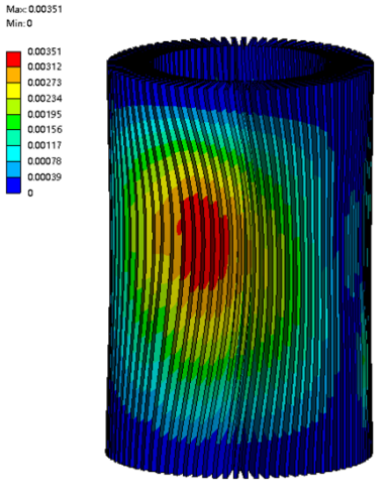


Figure 10. Deformation diagram of the filter element.

4.5.4. Simulation Data Analysis

By analyzing the simulation data from the fluid–structure coupling simulation, it is clear that the pressure drop of the original structure of the HDT air filter was 2.20 kPa, and the pressure loss of the overall structure was large. The uneven pressure distribution of the filter element will affect the filter efficiency. When the filter element is impacted by high-speed fluid for a long time, its deformation increases. This shortens the service life of the filter element and affects the normal operation of the engine. Therefore, structural optimization is required.

5. Structural Optimization

Based on the aforementioned numerical simulation of the flow characteristics of the air filter, structural optimization was carried out by changing the position of the air inlet duct, the number of pleats, and the height of the pleats of the air filter. This can help to reduce the overall pressure drop of the air filter and the deformation of the filter element under the action of the flow field.

5.1. Intake Duct Location Optimization

The housing of the air filter for HDTs comprises upper and lower parts. The total length of the upper casing was 295 mm, and the diameter of the intake duct was 120 mm. After considering the length relationship between the air filter housing and the intake duct, the position of the intake duct in the original structure of the HDT air filter was set as the initial value, and the intake duct was shifted down along the upper housing by 42 mm, 84 mm, 126 mm, and 168 mm, where numerical simulations were carried out. Figure 11 shows a schematic of the pressure drop of the average pressure at the inlet and outlet of the air filter under different flow rates as a function of the position of the intake duct. This figure shows that when the intake duct moved down from the original position along with the housing, the overall pressure drop of the air filter exhibited a trend of first decreasing and then increasing. When the position of the intake duct was moved down by 126 mm, the pressure drop of the air filter under different flow rates reached its lowest value. Figure 12 shows the overall pressure distribution of the air filter when the rated flow rate was 840 m^3/h. When the position moved down by 126 mm, the overall pressure value of the air filter decreased significantly, and the pressure distribution was more uniform. Therefore, the impact of the fluid flow on the housing was reduced.

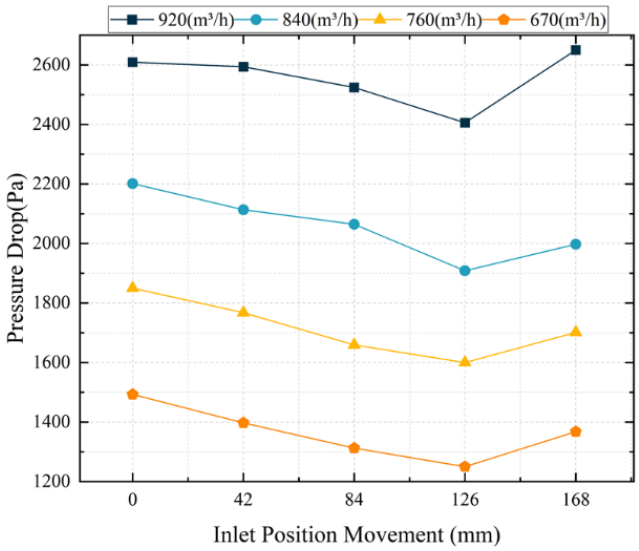


Figure 11. Variation in the air filter pressure drop with intake position at different flow rates.

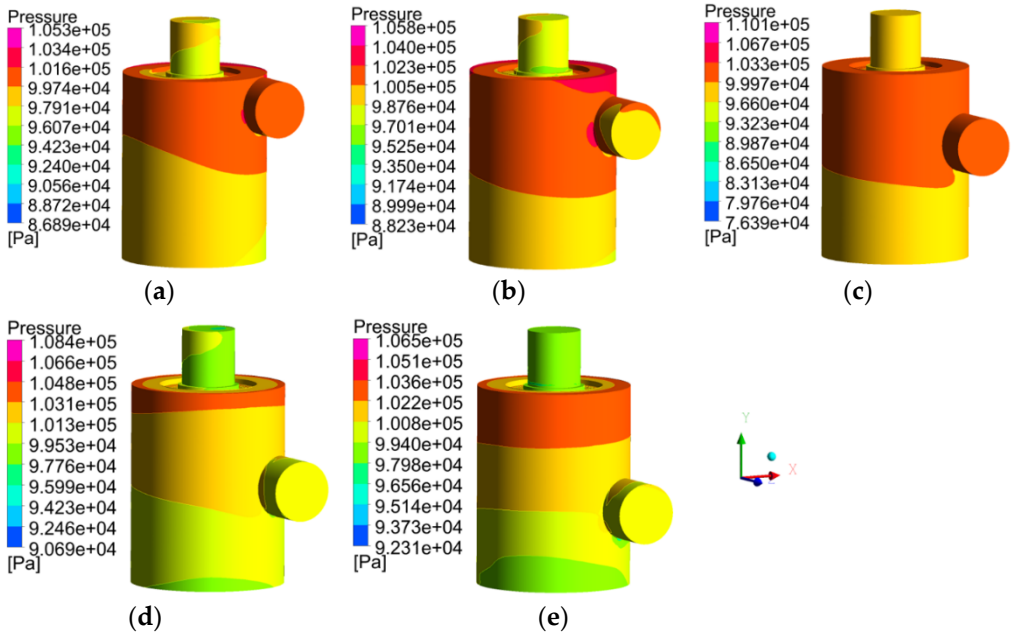
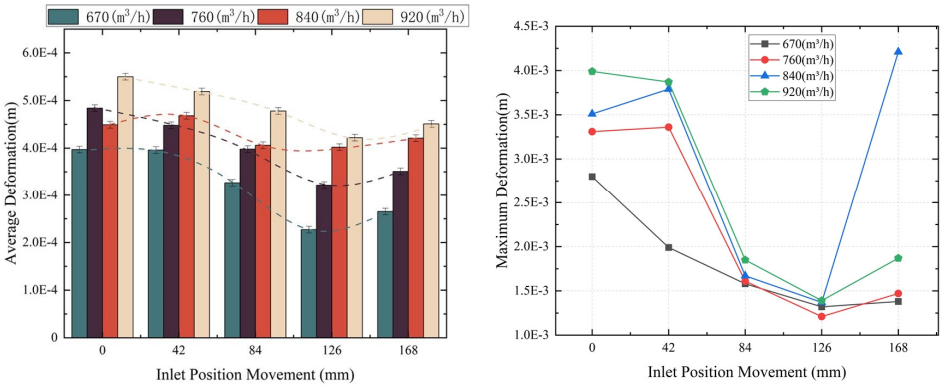


Figure 12. Overall pressure distribution of the air filter at a flow rate of 840 m^3/h. (**a**) y = 0 mm. (**b**) y = 42 mm. (**c**) y = 84 mm. (**d**) y = 126 mm. (**e**) y = 168 mm.

In addition to the pressure drop of the air filter, the flow uniformity of the filter element is also very important. In this study, the maximum deformation and average deformation parameters of the filter element were used to analyze the flow uniformity of the filter element under different schemes, the results of which are shown in Figure 13. This figure shows that the maximum deformation and average deformation of the filter element were also related to the position of the intake duct; under different flow conditions, the overall change trend of the filter element deformation was the same as that of the pressure drop. Taking the rated flow rate of 840 m^3/h as an example, when the intake duct moved down 126 mm in the direction of the housing, the maximum deformation of the filter element was reduced from 3.51×10^{-3} m for the original structure to 1.40×10^{-3} m, and the average deformation was also reduced from 4.49×10^{-4} m to 4.02×10^{-4} m. The decrease in the maximum deformation showed that the flow uniformity of the filter element was improved; however, the average deformation of the filter element did not change obviously, and thus, there is still room for improvement in the optimization of the air filter.



(**a**) (**b**)

Figure 13. Variation in the filter element deformation with intake position at different flow rates. (**a**) Average deformation. (**b**) Maximum deformation.

5.2. Optimization of the Pleat Count and Height of the Filter Elements

In this study, to further analyze the working performance of the HDT air filter, the filter element height and the number of pleats of the filter element were increased or decreased in equal proportion within the limited space in the air filter given that the intake duct position was moved down 126 mm from the original structure. The number of pleats of the original air filter element was 80 folds, and the filter element height was 277 mm. According to the actual working requirements, the filter element pleats were set to 60 folds, 70 folds, 80 folds, 90 folds, and 100 folds, and the filter element heights were 257 mm, 267 mm, 277 mm, 287 mm, and 297 mm. The pleat number and the height of the filter element were simulated simultaneously; that is, the pleat number and the height of the filter element changed at the same time, and the variation law of the pressure drop at the inlet and outlet of the air filter was obtained, as shown in Figure 14.

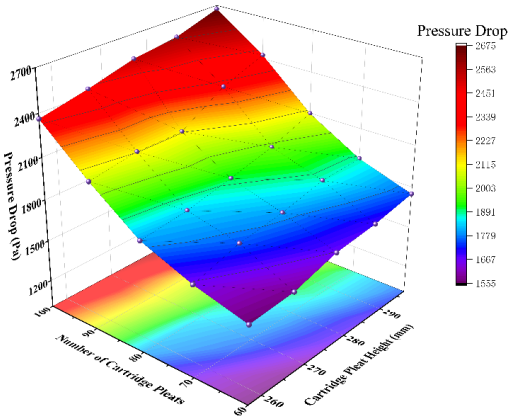


Figure 14. Variation of pressure drop with the number of pleats and filter element height.

It can be seen from Figure 14 that with an increase in the pleat number and filter element height of the air filter, the filtering area of the air filter increased and the pressure drop of the air filter also increased; however, the nonlinearity increased proportionally. The functional relationship between the pressure drop and the number of pleats and filter element height was obtained via surface fitting as follows:

$$Z = 6089.03 - 57.59X - 26.46Y + 0.34X^2 + 0.047Y^2 + 0.089XY \quad (12)$$

where the independent variable X is the pleat number of the filter element, the independent variable Y is the height of the filter element, and the dependent variable Z is the pressure drop.

When the number of pleats of the filter element was greater than 80 folds, the pressure drop rose sharply. As the pleat spacing decreased, the viscous frictional resistance between the pleats and the fluid increased with an increase in the number of pleats, and the pressure drop also increased rapidly. From the perspective of the pressure drop loss, when the filter element height was low, the resulting pressure drop value was also lower; however, the filter area became smaller as the filter element height decreased, which affected the intake air volume of the engine, the oil–gas ratio of the engine, and the turbulent flow intensity of the inner cavity of the air filter. Therefore, an air filter with a lower pressure drop should be used to maintain the filtering effect. When the number of pleats of the filter element was between 60 and 80 folds and the height of the filter element was 257 mm to 277 mm, the pressure drop of the air filter was low; these values could be used as the selection ranges of the filter element.

Figure 15 shows the variation of the deformation of the filter element with the pleat number and filter element height based on the fluid–structure interaction simulation. It can be seen from Figure 15 that the change trend of the average deformation of the filter element was consistent with the change trend of the pressure drop; that is, as the pleat number and filter element height increased, the deformation also increased. The increase in the number of pleats and the height of the filter elements shortened the gap between the pleats, increasing the pressure exerted by the fluid flow on the filter element, making the filter element more prone to deformation. The average deformation of the filter element was reduced; that is, the deformation of the filter element in the circumferential direction was more uniform, the influence of the filter element deformation on the flow field was reduced, and the generation of eddy currents was reduced. This can improve the working efficiency of the filter element and prolong its service life. As the number of pleats increased, the maximum deformation of the filter element exhibited a trend of increasing gradually. However, when the number of pleats of the filter element was 90 folds, the filter element at all pleat heights exhibited a peak value of the maximum deformation amount. There was no linear relationship with the magnitude of the filter element height. When the height was 267 mm, the maximum deformation amount was 5.80×10^{-3} m, which was related to the complex flow field in the air filter. The relationship between the maximum deformation of the filter element and the filter element height was not obvious. When the number of pleats was less than 80 folds, the maximum deformation of the filter element with different heights was maintained stably between 2.0×10^{-3} m and 3.0×10^{-3} m. When the height of the filter element was 267 mm and the number of pleats was 60 folds or 70 folds, the maximum deformation of the filter element was the smallest.

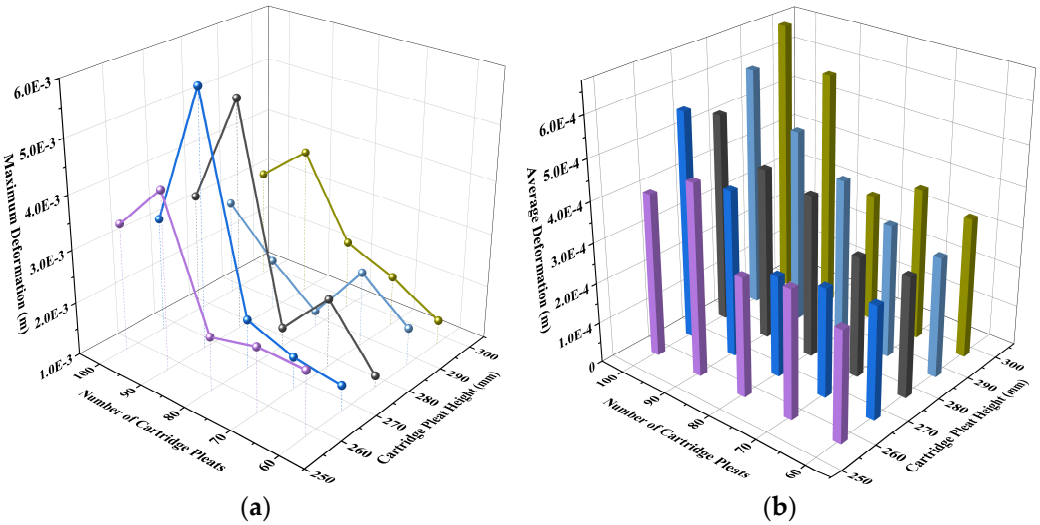


Figure 15. Variation of filter element deformation with pleat number and filter element height. (**a**) Maximum deformation. (**b**) Average deformation.

5.3. Optimization Results

According to the abovementioned analysis, after comprehensively considering factors such as the pressure drop, filter element deformation, and filtration area, an improvement plan for HDT air filters was finally determined: the intake duct was moved down from the original position by 126 mm, the height of the filter element was set to 267 mm, and the pleat number of the filter element was 70 folds. The parameters before and after the optimization of the air filter are shown in Table 3, which shows that the optimized air filter reduced the pressure drop by 445 Pa in comparison to the original structure, the maximum deformation of the filter element was reduced by 54.1%, and the average deformation was reduced by 39.8%.

Table 3. Comparison of the parameters before and after the optimization of the HDT air filter.

System Status	Pleat Number	Filter Height (mm)	Pressure Drop (Pa)	Maximum Deformation (m)	Average Deformation (m)
Before	80	277	2201.2	3.51×10^{-3}	4.49×10^{-4}
After	70	267	1756.2	1.61×10^{-3}	2.70×10^{-4}

Figure 16 shows a comparison of the pressure distributions before and after the optimization; the internal pressure value of the air filter was reduced overall, the pressure distribution in the circumferential direction of the filter element was more uniform, and the pressure on the housing was also reduced, reducing its wear. Figure 17 shows the velocity distribution before and after the optimization. Although the air still directly impacted the left filter element after entering the air filter, the fluid velocity in the high-speed area was significantly reduced. The overall impact of the filter element was weakened by the fluid, which improved the flow uniformity on the circumference of the filter element, reaching the optimization goal.

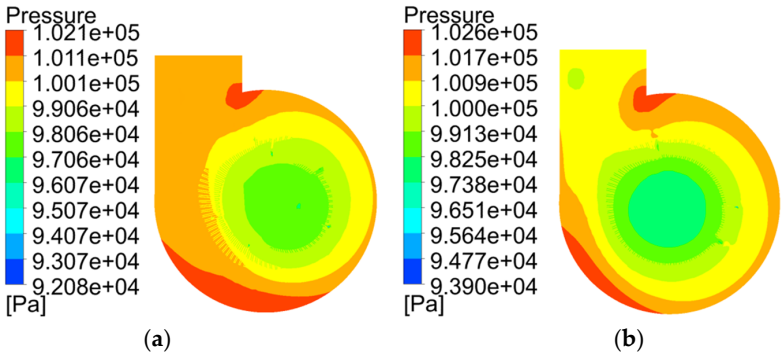


Figure 16. Pressure distribution diagram before and after the air filter optimization. (**a**) Before optimization. (**b**) After optimization.

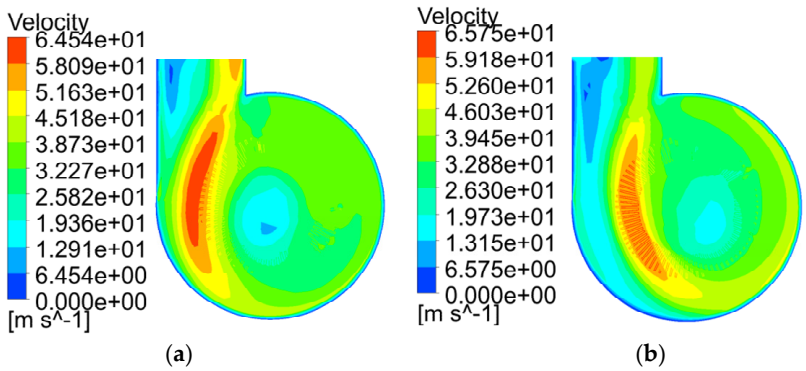
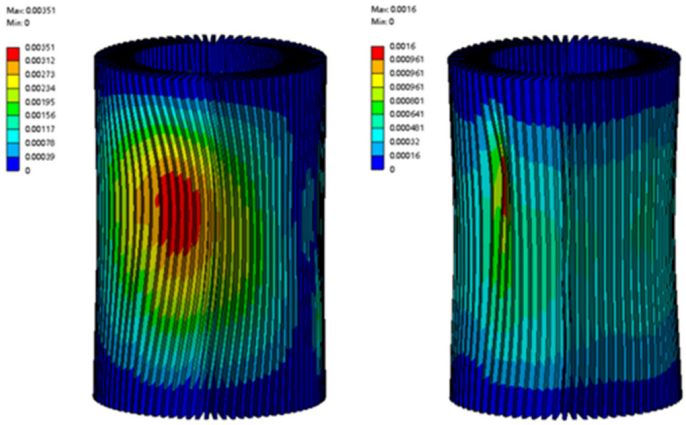


Figure 17. Velocity distribution diagram before and after the air filter optimization. (**a**) Before optimization. (**b**) After optimization.

Figure 18 shows the deformation diagram of the filter element under the action of fluid–structure coupling before and after the optimization. It can be seen from this figure that the overall deformation of the filter element was significantly improved, and the local high deformation area was reduced. The maximum deformation was only 45.9% of the original structure, and the average deformation was also reduced to 60.1% of the original structure. The force of the filter element under the action of the flow field was uniform, the overall structure was stable, the gas circulation of the filter element was strengthened, and the filtration efficiency of the filter element was improved; therefore, the optimization of the air filter was realized.



(**a**) (**b**)

Figure 18. Filter deformation before and after the optimization. (**a**) Before optimization. (**b**) After optimization.

6. Test Equipment and Results

6.1. Test Results

Based on ISO-5011 (Air Filters for Internal Combustion Engines and Air Compressors–Performance Test), a TOCEIL type air filter comprehensive performance test bench was used to conduct experimental research on the air filter, and the pressure drop of the air filter (pressure drop), original filtration efficiency, coarse filtration efficiency, cumulative efficiency, dust-holding capacity, and other parameters were tested. The test bench is shown in Figure 19.



(**a**) (**b**)

Figure 19. Air filter comprehensive performance test bench. (**a**) Physical drawing of test-bed. (**b**) Air filter pressure drop test.

The dust used in the coarse filtration efficiency test was the American PTI test dust ISO12103-A2, and 270 mesh quartz sand was used in the dust capacity test, as shown in Figure 20.



(**a**) (**b**)

Figure 20. Test dust. (**a**) ISO12103-A2. (**b**) 270 mesh quartz.

During the test, the data of the air volume flow, pressure difference, static pressure, pressure drop, and dust-holding capacity were corrected according to the standard conditions; that is, the atmospheric pressure was 100,300 Pa and the temperature was 22 °C. The test results of the HDT air filter are shown in Tables 4 and 5.

Table 4. HDT air filter pressure drop test results.

Flow (m^3/h)	510	590	670	760	840	920
Pressure drop (kPa)	0.91	1.19	1.49	1.87	2.25	2.68

Table 5. HDT air filter filtration efficiency test results.

Raw Filtration Efficiency (%)	**Dust Pre-Filter Efficiency (%)**	**Filtration Efficiency (%)**	**Dust-Holding Capacity (g)**
99.6	41.67	99.99	1297.87

6.2. Comparisons of the Simulation Results and Test Results

In this study, CFX software was used for the simulation; it was used to simulate and calculate the static pressure difference between the inlet and outlet of the original model under different outlet flow rates, allowing us to obtain the pressure drop value of the air filter, which was compared with the data in the test results, as shown in Table 6.

Table 6. Comparison of the pressure drop results.

Flow (m^3/h)	510	590	670	760	840	920
Test result (kPa)	0.91	1.19	1.49	1.87	2.25	2.68
Calculation result (kPa)	0.89	1.17	1.44	1.85	2.20	2.61
Error (%)	1.1	1.7	3.4	1.1	2.3	2.6

From the comparison in Table 6, it can be seen that the pressure drop values obtained from the test were larger than the pressure drop values obtained from the simulation, which was due to the influence of many external factors, such as the air humidity. The air humidity leads to greater friction between the air and the inner wall surface of the air filter, resulting in larger values in the pressure drop.

The data in Table 6 are compared and analyzed in Figure 21. It can be seen that the experimental results and simulation results based on fluid–structure coupling exhibited very small errors, with an error range of less than 4%, which could be controlled to below 3%. In addition, the growth rates of the two sets of data were almost the same, and the

error did not increase with the increase in the flow rate. From the results, it was clear that the simulation research method used in this study had higher accuracy when simulating the actual working conditions of the HDT air filter, providing a reliable guarantee for the structural optimization of the air filter.

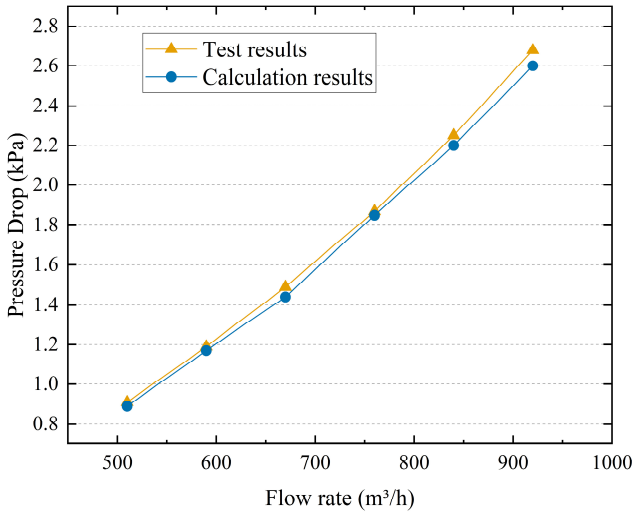


Figure 21. Comparison of the simulation results and experimental results.

7. Conclusions

In this study, according to the actual structure and working environment of an HDT air filter, the porous media model was used to simulate the filtration process of the filter element in the flow field, and the DPM model was used to understand the movement process of the particles in the flow field. Based on this, a simulation method was constructed, where the filter element part simultaneously participated in the fluid domain calculation as a porous medium region and participated in the fluid–structure coupling calculation as a solid domain. This helped with investigating the influence of fluid flow on the filter element and analyzing the reasons for increased deformation and wear on the filter element, which helped to reflect the actual working conditions in an air filter. The conclusions drawn from this study are summarized as follows:

(1) The simulation analysis method based on fluid–structure interaction and discrete phase model was suitable for the study of an HDT air filter. When comparing the pressure drop numerical simulation results with the test results, the error of the results under six different air flow rates was found to be basically less than 3%, and the maximum error was 3.4%. Compared with traditional simulation methods, the simulation accuracy was improved.

(2) Due to the irregularity of the fluid flow inside the air filter, the filter element was prone to large deformation in a certain direction (maximum deformation reached 3.51 mm), which will accelerate the mechanical damage (breaking, rupturing) of the filter element.

(3) The results of structural optimization showed that when the position of the intake duct moved down from the initial position along the housing, the pressure drop of the air filter showed a trend of first decreasing and then increasing. When the position of the intake pipe moved down 126 mm from the original position (the intake pipe was basically parallel to the lower end of the filter element), the pressure drop of the air filter under different flow rates reached the minimum value and the pressure decreased on average by 252 Pa. Taking the rated flow rate of 840 m^3/h as an example, when the intake duct moved down 126 mm in the direction of the housing, the maximum deformation of the filter element is reduced from 3.51×10^{-3} m for the original structure to 1.40×10^{-3} m, and the average deformation was also reduced from 4.49×10^{-4} m to 4.02×10^{-4} m.

(4) As the number of pleats increased, the maximum deformation of the filter element basically showed a gradually increasing trend. However, when the number of pleats of

the filter element was 90 folds, the maximum deformation peaks of the filter elements of different heights appeared. There was no linear relationship between the size of the peak and the height of the filter element.

(5) After comprehensively considering factors such as the air intake resistance, filter element deformation, and filter area of HDT air filters, the final optimization plan was as follows: the position of the intake duct was moved downward by 126 mm from the original direction and the filter element was improved by having a height of 267 mm and a pleat number of 70 folds. At the rated flow rate of 840 m^3/h, compared with the original structure, the pressure was reduced by 445 Pa, the maximum deformation of the filter element was reduced by 54.1%, and the average deformation was reduced by 39.8%.

The simulation method presented in this paper can be applied to research in the truck industry in terms of factors such as flow stability, vibration, and noise. In order to realize the sustainable development of the ecological environment and reduce the pollution of heavy-duty trucks, the optimization method used in this study can be applied to actual industrial production. In the future, a simulation study on the influence of the air filter on the engine power and emissions of a heavy-duty truck can be carried out.

Author Contributions: Conceptualization, X.S.; Methodology, X.S. and P.H.; Software, P.H.; Supervision, F.C. and W.R.; Validation, W.R.; Writing—original draft, X.S.; Writing—review & editing, F.C. All authors have read and agreed to the published version of the manuscript.

Funding: This research was funded by the Natural Science Foundation of Shandong Province of China (grant no. ZR2021ME235), the Innovation Team Project of Ji'nan (grant no. 2019GXRC035), and the Key Research and Developmental Program of Shandong Province of China (grant no. 2019GGX104104).

Institutional Review Board Statement: Not applicable.

Informed Consent Statement: Not applicable.

Data Availability Statement: Data are contained within the article.

Conflicts of Interest: The authors declare no conflict of interest.

References

1. Marco, B. Development of an Air Filtration Software. *SAE Int. J. Mater. Manuf.* **2014**, *7*, 300–307.
2. Dziubak, T.; Karczewski, M. Experimental Study of the Effect of Air Filter Pressure Drop on Internal Combustion Engine Performance. *Energies* **2022**, *15*, 3285. [CrossRef]
3. Amiri, H.A.A.; Hamouda, A.A. Pore-scale modeling of non-isothermal two phase flow in 2D porous media: Influences of viscosity, capillarity, wettability and heterogeneity. *Int. J. Multiph. Flow* **2014**, *61*, 14–27. [CrossRef]
4. Kang, J.H.; Ih, J.G. Acoustical Characteristics of the Air Filter in the Engine Intake Air Cleaner. *Int. J. Automot. Technol.* **2018**, *19*, 981–991. [CrossRef]
5. Rebai, M.; Prat, M.; Meireles, M.; Schmitz, P.; Baclet, R. A semi-analytical model for gas flow in pleated filters. *Chem. Eng. Sci.* **2010**, *65*, 2835–2846. [CrossRef]
6. Butt, Q.R.; Bhatti, A.I.; Mufti, M.R.; Rizvi, M.A.; Awan, I. Modeling and online parameter estimation of intake manifold in gasoline engines using sliding mode observer. *Simul. Model. Pract. Theory* **2013**, *32*, 138–154. [CrossRef]
7. Rahman, M.M.; Kamil, M.; Bakar, R.A. Engine performance and optimum injection timing for 4-cylinder direct injection hydrogen fueled engine. *Simul. Model. Pract. Theory* **2011**, *19*, 734–751. [CrossRef]
8. Li, Q.; Wang, Z.C.; Shao, S.Q.; Niu, Z.Q.; Xin, Y.L.; Zhao, D.; Hou, Y.Y.; Xu, Z.W. Experimental study on the synthetic dust loading characteristics of air filters. *Sep. Purif. Technol.* **2022**, *284*, 11. [CrossRef]
9. Yun, J.E. Optimal Design of Off-Road Utility Terrain Vehicle Air Filter Intake. *Energies* **2021**, *14*, 2269. [CrossRef]
10. Birtok-Baneasa, C.; Ratiu, S.A.; Alexa, V.; Craciun, A.L.; Josan, A.; Budiul-Berghian, A. Reducing Emissions by Using Special Air Filters for Internal Combustion Engines. In Proceedings of the Conference on Innovative Ideas in Science, Baia Mare, Romania, 10–11 November 2016; Iop Publishing Ltd.: Baia Mare, Romania.
11. Wang, G.; Teng, M.A.; Liang, X.; Meimei, L.I.; Zhang, W. The CFD Analysis and Structure Optimization of Vehicle-used Desert Swirl Tube Air Coarse Filter. In Proceedings of the 2nd National Conference on Information Technology and Computer Science (CITCS 2015), Faridabad, India, 18–19 October 2013.
12. Allam, S.; Elsaid, A.M. Parametric study on vehicle fuel economy and optimization criteria of the pleated air filter designs to improve the performance of an I.C diesel engine: Experimental and CFD approaches. *Sep. Purif. Technol.* **2020**, *241*, 18. [CrossRef]

13. Pradhan, A.K.; Das, D. A comparative study on filtration performance of mono-, bi-, and multi-constituent nonwoven air filter media. *J. Text. Inst.* **2018**, *109*, 1521–1527. [CrossRef]
14. Maddineni, A.K.; Das, D.; Damodaran, R.M. Numerical investigation of pressure and flow characteristics of pleated air filter system for automotive engine intake application. *Sep. Purif. Technol.* **2019**, *212*, 126–134. [CrossRef]
15. Dziubak, T.; Bakala, L.; Karczewski, M.; Tomaszewski, M. Numerical research on vortex tube separator for special vehicle engine inlet air filter. *Sep. Purif. Technol.* **2020**, *237*, 14. [CrossRef]
16. Rieger, M.; Hettkamp, P.; Lhl, T.; Madeira, P. Efficient Engine Air Filter for Tight Installation Spaces. *ATZ Heavy Duty Worldw.* **2019**, *12*, 56–59. [CrossRef]
17. Naqvi, S.B.; Bottaro, A. Interfacial conditions between a free-fluid region and a porous medium. *Int. J. Multiph. Flow* **2021**, *141*, 103585. [CrossRef]
18. Saini, A.K.; Chauhan, S.S.; Tiwari, A. Creeping flow of Jeffrey fluid through a swarm of porous cylindrical particles: Brinkman–Forchheimer model. *Int. J. Multiph. Flow* **2021**, *145*, 103803. [CrossRef]
19. De Nayer, G.; Breuer, M.; Boulbrachene, K. FSI simulations of wind gusts impacting an air-inflated flexible membrane at Re = 100,000. *J. Fluids Struct.* **2022**, *109*, 103462. [CrossRef]
20. Ahn, S.; Shim, E.; Kim, Y.; Bae, Y.-S.; Eom, H. Air filtration performance enhancement of PTFE foam–coated filters at high temperatures via secondary strongly adhering PTFE nanofiber coatings. *Process Saf. Environ. Prot.* **2022**, *162*, 914–922. [CrossRef]
21. Al-Sarkhi, A.; Chambers, F.W. Optimization technique for design of automotive air filter Housings with improved fluid dynamic performance and filtration. *Part. Sci. Technol.* **2004**, *22*, 235–252. [CrossRef]
22. Zhao, S.; Jiang, A. Optimization of a Engine Air Filter by CFD. *Mach. Des. Manuf.* **2015**, *294*, 163–166.
23. Li, R. *Study on Simulation and Test Technology of Air Filter's Performace with Scavenged System*; Zhejiang University: Hangzhou, China, 2017.
24. De Bartolo, C.; Algieri, A.; Bova, S. Simulation and experimental validation of the flow field at the entrance and within the filter housing of a production spark-ignition engine. *Simul. Model. Pract. Theory* **2014**, *41*, 73–86. [CrossRef]
25. Lu, J.; Li, J.; Sun, Y.; Chen, K.; Qiao, M.; Li, W. The Performance Simulation and Experiment of Air Filter of Armored Vehicle in Plateau Environment. *Acta Armamentarii* **2015**, *36*, 1556–1561. [CrossRef]
26. Liu, W.; Long, Z.W.; Chen, Q.Y. A procedure for predicting pressure loss coefficients of duct fittings using computational fluid dynamics (RP-1493). *HvacR Res.* **2012**, *18*, 1168–1181. [CrossRef]
27. Li, J.; Liu, Z.-T.; Liu, Z.-M.; Tan, Y.-N.; Yu, X.-L. Simulation and test of flow process in air filte. *J. Zhejiang Univ. (Eng. Sci.)* **2012**, *46*, 6.
28. Fotovati, S.; Hosseini, S.A.; Tafreshi, H.V.; Pourdeyhimi, B. Modeling instantaneous pressure drop of pleated thin filter media during dust loading. *Chem. Eng. Sci.* **2011**, *66*, 4036–4046. [CrossRef]
29. Tan, Y.-N. *Simulation Analysis and Experimental Reasearch of Air Filter*; Zhejiang University: Hangzhou, China, 2010.
30. Binns, R.; Shollenberger, K.A.; Asme. Modeling Flow Across a Race Car Air Filter. In Proceedings of the 2nd US-European Fluids Engineering Division Summer Meeting, Miami, FL, USA, 17–20 July 2006; pp. 305–313.